Renormalization group analysis of competing orders and the pairing symmetry in Fe-based superconductors

A.V. Chubukov

Department of Physics, University of Wisconsin-Madison, Madison, WI 53706, USA

(Dated: February 24, 2009)

We analyze antiferromagnetism and superconductivity in novel $Fe-$based superconductors within the weak-coupling, itinerant model of electron and hole pockets near $(0,0)$ and (π, π) in the folded Brillouin zone. We discuss the interaction Hamiltonian, the nesting, the RG flow of the couplings at energies above and below the Fermi energy, and the interplay between SDW magnetism, superconductivity and charge orbital order. We argue that SDW antiferromagnetism wins at zero doping but looses to superconductivity upon doping. We show that the most likely symmetry of the superconducting gap is A_{1g} in the folded zone. This gap has no nodes on the Fermi surface but changes sign between hole and electron pockets. We also argue that at weak coupling, this pairing predominantly comes not from spin fluctuation exchange but from a direct pair hopping between hole and electron pockets.

I. INTRODUCTION

Recent discovery of superconductivity (SC) in the iron-based layered pnictides with T_c ranging between 26 and 52K generated enormous interest in the physics of these materials, which also hold hold strong potential for applications. [1]. SC has been observed in oxygen containing 1111 systems RFeAsO, where R=La, Nd, Sm, Pr, Gd, in oxygen-free 122 systems AFe$_2$As$_2$, where A=Ba, Sr, Ca, and in several other classes of materials like LiFeAs with 111 structure and α-FeSe with 11 structure [2,3,4,5,6,7,8].

In several respects, the pnictides are similar to the cuprates. Like the cuprates, the pnictides are highly two-dimensional, their parent materials show antiferromagnetic long-range order below 150K[2,9,10,11,12], and superconductivity occurs upon doping of either electrons[2,3,4,5] or holes[6] into FeAs layers. This lead to early conjectures that the physics of the pnictides is similar to that of the cuprates and involves insulating Mott behavior.[13,14,15,16] Resistivity measurements, however, showed that iron pnictides remain itinerant down to zero doping, although the jury is still deliberating whether some signatures of Mott physics have been observed at higher energies (see e.g., [16,17]). Other evidences for itinerant behavior include

- a relatively small value of the observed magnetic moment per Fe atom in the magnetically ordered phase – $12 - 16\%$ of $2\mu_B$ in 1111 materials[10,12].

- a good agreement between electronic band structure calculations[18,19,20,21,22,23] and ARPES and magneto-oscillation measurements of the Fermi surface (FS) and electronic states [24,25,26,27,28,29]

- Drude-like behavior of the optical conductivity at small frequencies[30]

Although there are certain variations in the crystal structure between different classes of pnictides, the low-energy electronic structure is likely the same for all systems and consists of two small hole pockets at the center of the Brillouin zone (BZ) and two small electron pockets centered around M points (Fig.1). The M points are located $q_1 = (0, \pi/a)$ and $q_2 = (\pi/a, 0)$ in the unfolded BZ (one Fe atom in the unit cell) and at identical points $k_1 = (\pi/\bar{a}, \pi/\bar{a})$ and $k_2 = (\pi/\bar{a}, -\pi/\bar{a})$ in the folded BZ (two Fe atoms in the unit cell, $\bar{a} = a\sqrt{2}$) (see Fig.2). The relations between the momenta in the folded and unfolded zones are $k_x = (q_x + q_y)/\sqrt{2}$, $k_y = (q_x - q_y)/\sqrt{2}$. The unfolded BZ includes only Fe states, the folded BZ (the correct zone) takes into account the fact that only a half of Fe states are actually identical in pnictides because of As which resides either above or below Fe plane (Fig.2). Below we will use the folded BZ. Throughout the paper we define M point as $\mathbf{Q} = (\pi/\bar{a}, \pi/\bar{a})$ and set $\bar{a} = 1$.

The goal of this paper is to summarize recent work done in collaboration with D. Efremov and I. Eremin[31] and by myself on the weak-coupling, Fermi-liquid analysis of magnetic and superconducting instabilities in the pnictides. I will address several issues:

- what interactions cause magnetism and SC?

- are SC and magnetism competing orders?

- is charge order possible?

- what is the symmetry of the SC gap and how to overcome intra-pocket repulsion

- is the pairing magnetically mediated?

Central to weak coupling analysis is the idea of a near-nesting between electron and hole pockets at zero doping. The nesting does not mean that any of the FS has parallel pieces but rather implies that, by moving a hole FS by $\mathbf{Q}$, one obtains a near-perfect match with an electron FS. This FS geometry is in a reasonable agreement with ARPES and magneto-oscillation measure-
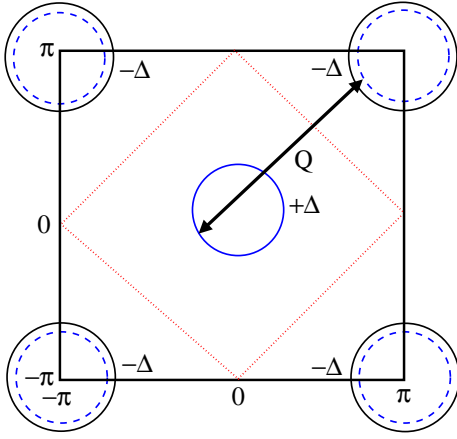
FIG. 1: (color online) A simplified geometry of $Fe-$based superconductors used in the present work. The Fermi surface consists of an electron pocket around (π,π) (black solid circle), and a hole pocket of roughly equal size around $(0,0)$ (blue solid circle). A near-perfect nesting between hole and electron pockets means that, by moving a hole FS by (π,π), one obtains a near-perfect match with an electron FS. Upon electron doping, the size of the electron pocket increases (dashed blue $\rightarrow$ black), what breaks the nesting. Upon hole doping, the size of a hole FS increases, what again breaks the nesting. $+\Delta$ and $-\Delta$ are the values of the superconducting gaps on the two FS for an s^+ superconducting state. (From Ref.[31].)
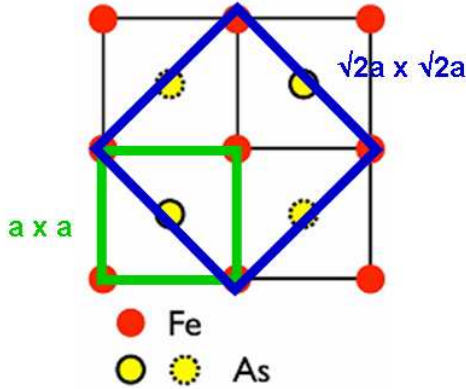

FIG. 2: (color online) Folded and unfolded BZ (courtesy of I. Eremin). Unfolded BZ is $a \times a$ square (one Fe atom per unit cell). Unfolded zone (the correct one) is constructed to take into account the fact that only a half of Fe states are actually identical because As, whose projection onto an Fe plane is at a center of a square, is located slightly above or below an Fe plane. The folded zone has two Fe atoms in the unit cell and is a square with dimensions $\sqrt{2}a \times \sqrt{2}a$, rotated by 45^0 compared to the unit cell in unfolded zone.

ments [24,25,26,27,28,29]. It has been known from the studies of chromium and its alloys in the 70th[32,33] and from generic theoretical studies of "excitonic insulators"[34] that such nesting leads to a spin-density-wave (SDW) order with momentum $\mathbf{Q}$ already at weak coupling in the same way as SC order appears at weak coupling in

a BCS superconductivity. For pnictides, the role of nesting for SDW order was emphasized by Cvetkovic and Tesanovic[35] and Barzykin and Gorkov[36]. Upon doping, either by holes or by electrons, one of the two pockets gets relatively larger and the nesting breaks down. In this situation, SDW order gets weaker[35,37,38,39], and at some doping superconductivity emerges. How pnictides evolve from a magnet to a superconductor is not clear at the moment, and there are experimental evidences for both first order and continuous transitions. Theoretically, both situations are possible.[40]

What interaction causes superconductivity and what is the symmetry of the superconducting gap are the two most intriguing issues for the pnictides. A conventional phonon-mediated s-wave superconductivity is an unlikely possibility because electron-phonon coupling calculated from first principles is quite small[41]. An electronic mechanism is therefore more likely. Mazin et al[21] conjectured, by analogy with the cuprates, that SC in pnictides is mediated by antiferromagnetic spin fluctuations. This pairing mechanism is most effective if the superconducting gap changes the sign under the momentum shift by $\mathbf{Q}$. For the cuprate FS, this unambiguously leads to $d_{x^2-y^2}$ superconductivity. For pnictides, the requirement is that the gap must change sign between hole and electron FS. This does not unambiguously determines the gap structure, but most natural would be the gap which is a constant Δ along a hole FS and a constant $-\Delta$ along an electron FS. In the classification of the eigenfunctions of the tetragonal D_{4h} group, this gap belongs to A_{1g} representation and is roughly $\Delta(\mathbf{k}) = \Delta(\cos k_x + \cos k_y)/2$[36]. We will refer to this gap symmetry as s^+. The s^+ gap has been found as the most likely candidate in some of the RPA studies based on a 5-orbital Hubbard model[42], a 2-band spin-fluctuation model[43], and in the renormalization group (RG) analysis[31,44] (see below). The s^+ gap structure also emerges in the analysis based on localized spin models[45].

There are. however, two potential problems with the spin-fluctuation mechanism. First, the close proximity to a magnetic phase does not a'priori guarantee that the pairing is magnetically mediated. This is particularly true for pnictides because of two separate FS in which case there are multiple interactions between hole and electron states, and the interaction which gives rise to magnetism is not necessary the same interaction that gives rise to SC. This has to be verified in the calculations. We will argue below that the full pairing interaction does have a component which represents the exchange by soft dynamic magnetic fluctuations peaked at $\mathbf{Q}$. However, we will argue that this component is subleading at weak coupling, and the dominant pairing component is a direct pair-hopping term. This does not change the outcome, though, that the pairing is in the s^+ channel.

Second, intra-pocket repulsion does not cancel out from the s^+ pairing problem because average gap along either hole or electron FS is non-zero. The intra-

pocket interaction term in the Hamiltonian is quite likely stronger than the pair-hopping term[31,44] such that at this level s^+ channel is repulsive. One has to see to where the interactions flow at small energies and whether the renormalized pair-hopping term eventually becomes larger than intra-pocket repulsion.

This flow of couplings is outside RPA in which the interactions have the same values as in the Hamiltonian.[46] Whether or not s^+ superconductivity is favored in RPA then likely depends on the values of the bare interactions in the underlying 5-orbital model (intra-and inter-orbital Hubbard interactions, intra-orbital exchange and pair-hopping terms). While some researchers found the s^+ state[42], others[37] found that more likely candidates are two nearly degenerate states in which the gap has nodes on one of the FS sheets and no nodes on the other. One such state is another extended s-wave state with $\Delta(\mathbf{k}) \approx \Delta \cos \frac{k_x}{2} \cos \frac{k_y}{2}$, the second is $d_{x^2-y^2}$ state with $\Delta(\mathbf{k}) \approx \Delta \sin \frac{k_x}{2} \sin \frac{k_y}{2}$. In the unfolded BZ, these two are $\cos q_x + \cos q_y$ and $\cos q_x - \cos q_y$, respectively (see Ref.[36]). These two states transform into each other under the translation by $\mathbf{Q}$, but are decoupled in the gap equation. The extended s-wave state with $\Delta(\mathbf{k}) \propto \cos \frac{k_x}{2} \cos \frac{k_y}{2}$ is not orthogonal to $\Delta(\mathbf{k}) \propto \cos k_x + \cos k_y$ as both are members of the A_{1g} representation of D_{4h} group. However, for small hole and electron pockets, the matrix element between $\cos k_x + \cos k_y$ and $\cos k_x/2 \cos k_y/2$ states is small, and the two can be treated "almost" independently.

The gaps with $\Delta(k) \propto \cos \frac{k_x}{2} \cos \frac{k_y}{2}$ and $\Delta(k) \propto \sin \frac{k_x}{2} \sin \frac{k_y}{2}$ are less sensitive to intra-pocket repulsion as the average of $\Delta(k)$ along one of the FS sheets is zero, and win within RPA over $\cos k_x + \cos k_y$ state when intra-pocket repulsion is the strongest interaction. On the other hand, these two states are less favorable candidates once we include inter-pocket attraction because the magnitude of one of the gaps at the FS is small, of order k_F^2. Other pairing states, like d_{xy} states in the folded BZ with $\Delta(\mathbf{k}) = \Delta \sin k_x \sin k_y$ have also been proposed[38] and are favored in a parameter range in which the pairing interaction is peaked at momenta smaller than $2k_F$.

From experimental perspective, the issue of the gap symmetry is also unsettled. ARPES[24,25,26,27] and Andreev spectroscopy[47] measurements have been interpreted as evidence for a nodeless gap, either a pure s-wave gap or an s^+ gap. The resonance observed in neutron measurements below T_c[48] is consistent with an s^+ gap[39,49] but not with a pure s−wave gap or $\cos \frac{k_x}{2} \cos \frac{k_y}{2}$ or $\sin \frac{k_x}{2} \sin \frac{k_y}{2}$ gaps. On the other hand, nuclear magnetic resonance (NMR) data [50,51,52] and some of the penetration depth data[53,54] were interpreted as evidence for the nodes in the gap. Some, but not all of these data can still be reasonably fitted by a model of an s^+ SC with ordinary impurities[31,43,55,56,57]. Several groups[58,59,60] suggested specific measurements which could potentially unambiguously distinguish between different pairing symmetries.

In the bulk of the paper we discuss weak-coupling approach to the pnictides. The most essential results of our calculations are

- magnetism and SC emerge due to the interplay between pair hopping and inter-pocket forward scattering

- magnetism and SC are competing orders; magnetism wins for perfect nesting but looses to SC upon doping

- orbital charge order appears at T only slightly below magnetic ordering temperature

- the pairing symmetry is s^+, intra-pocket repulsion is not an obstacle, at least when k_F is small

- pairing interaction is *not* magnetically mediated – it predominantly comes from a direct pair hopping between hole and electron FS

Weak-coupling approach is certainly only a first step in the understanding of the physics of the pnictides and should be followed by more involved calculations which include the dynamics of the interactions. These dynamic calculations should allow one to understand what sets the upper cutoffs for the effective interactions in density-wave and pairing channels, to obtain the numbers for T_N and T_c, and to study quantitatively the behavior of various observables. Only after that one should be able to settle the issue whether weak/moderate coupling approach to the pnictides captures most of the physics, or strong coupling effects associated with Mott physics are also essential.

The paper is organized as follows. In Sec.II we introduce the model and discuss the approximations. In Sec.III we discuss renormalization group flow first at energies above E_F and then at energies below E_F. We show that RG equations are different in the two regions. In Sec.IV we discuss density-wave and pairing instabilities and address the issues whether magnetism and superconductivity are competing orders, can a charge density-wave order emerge, and is there a symmetry between different orders. In Sec.V we discuss whether the pairing can be viewed as mediated by spin fluctuations. In Sec.VI we present the conclusions.

II. THE LOW-ENERGY MODEL

We model iron pnictides by an itinerant electron system with two hole pockets centered at $(0, 0)$ and two electron pockets centered at $\mathbf{Q} = (\pi, \pi)$ in the folded BZ. We assume that the interactions do not distinguish between the two hole FS (and between the two electron FS) and restrict with one hole and one electron FS adding combinatoric factors to the interaction effects whenever necessary. There are fine magnetic effects associated with two

rather and one hole (and electron) FS[44,61] but we will not discuss them here.

There are three key assumptions of our weak-coupling approach to the pnictides.

- We assume that the interactions are small compared to the bandwidth such that the low-energy physics is determined solely by fermions with momenta near $(0,0)$ and $\mathbf{Q}$. The alternative description in terms of lattice spin models (like $J_1 - J_2$ model[13,16,17,61,62]) is valid if the interaction is comparable or stronger than the bandwidth.

- We assume that there is near-nesting between electron and hole pockets (by moving a hole FS by $\mathbf{Q}$ one obtains a near-perfect match with an electron FS). Nesting does not have to be perfect, but a typical energy associated with non-nesting should be smaller than the Fermi energy E_F.

- We assume that both hole and electron pockets are small compared to the size of the BZ. In energy units, this implies that the Fermi energy is much smaller than W.

The last two assumptions are at least partly consistent with ARPES and magneto-oscillation experiments and with band theory which all show that there is a near-nesting between at least one hole and one electron pockets, and also that both pockets are small and the Fermi energies (top of the band for hole pocket and bottom of the band for electron pocket) are of order $0.1eV$, much smaller than the bandwidth W, which is roughly $2eV$. The smallness of E_F compared to W is important for

our description because it opens up a relatively large energy window between W and E_F in which, on one hand, a low-energy description of nested electron and hole pockets is still valid, and, on the other hand, it is unimportant where precisely a fermion resides near one of the FS. We show below that in this particular regime, particle-hole and particle-particle channels of fermionic interaction become degenerate, and all five relevant couplings flow logarithmically under parquet RG.

The actual situation is indeed more complex than our simlified model. In particular, ARPES data show that there are two roughly equivalent electron pockets, but only one small hole pocket of about the same size[24,25,26,27]. The other hole pocket is larger in size, and the superconducting gap along this pocket is about two times smaller than the gap along the smaller hole pocket. Theoretical calculations[18,19,20,21,22,23,36] also show a somewhat more complex electronic structure, with another, fifth band in a close proximity to a Fermi level.

We label fermions near $(0,0)$ as $c-$fermions and fermions near $\mathbf{Q}$ as f-fermions. We assume that they have a parabolic dispersion

$$\epsilon_p^c = E_F - \frac{p^2}{2m}, \quad \epsilon_{p+Q}^f = \frac{(p+Q)^2}{2m} - E_F. \quad (1)$$

For convenience, we shift momenta of $f-$fermions by $\mathbf{Q}$ such that $\epsilon_p^f = -\epsilon_p^c$. In 2D, fermionic density of states is energy independent and we will use this in the RG analysis.

There are five different interactions involving $c-$ and $f-$ fermions

$$H = U_1^{(0)} \sum c_{\mathbf{p}_3\sigma}^\dagger f_{\mathbf{p}_4\sigma'}^\dagger f_{\mathbf{p}_2\sigma'} c_{\mathbf{p}_1\sigma} + U_2^{(0)} \sum f_{\mathbf{p}_3\sigma}^\dagger c_{\mathbf{p}_4\sigma'}^\dagger f_{\mathbf{p}_2\sigma'} c_{\mathbf{p}_1\sigma}$$

$$+ \frac{U_3^{(0)}}{2} \sum \left[f_{\mathbf{p}_3\sigma}^\dagger f_{\mathbf{p}_4\sigma'}^\dagger c_{\mathbf{p}_2\sigma'} c_{\mathbf{p}_1\sigma} + h.c \right] + \frac{U_4^{(0)}}{2} \sum f_{\mathbf{p}_3\sigma}^\dagger f_{\mathbf{p}_4\sigma'}^\dagger f_{\mathbf{p}_2\sigma'} f_{\mathbf{p}_1\sigma} + \frac{U_5^{(0)}}{2} \sum c_{\mathbf{p}_3\sigma}^\dagger c_{\mathbf{p}_4\sigma'}^\dagger c_{\mathbf{p}_2\sigma'} c_{\mathbf{p}_1\sigma} \quad (2)$$

The momentum conservation is assumed in all terms.

We label the couplings with subindex $''0''$ to emphasize that these are bare couplings. The terms with $U_4^{(0)}$ and $U_5^{(0)}$ are intraband interactions, the terms with $U_1^{(0)}$ and $U_2^{(0)}$ are interband interactions with momentum transfer 0 and $\mathbf{Q}$, respectively, and the term with $U_3^{(0)}$ is interband pair hopping. We show these interactions graphically in Fig.3. We approximate all five interactions by momentum-independent constants because of small sizes of hole and electron FS.

Below we will be using dimensionless interactions

$$u_i^{(0)} = U_i^{(0)} N_0 \quad (3)$$

where $N_0 = m/(2\pi)$ is the fermionic density of states.

Weak-coupling approach implies that $u_i^{(0)} < 1$.

Eq. (2) is the effective Hamiltonian for the interaction between low-energy fermions. It can be obtained, in principle, from the underlying five-orbital model[63] with intra-orbital and inter-orbital Hubbard interactions U and V and the Hund's rule coupling J. The relations between our U_i^0 and U, V, J should, however, be rather involved because all five Fe orbitals contribute to low-energy electronic states. The actual situation in pnictides is even more complex because Fe states also hybridize with As $p-$states[64].

Note that all vertices in Eq. (2) are δ-functions in spin indices, i.e., all bare interactions are in the charge channel. Bare spin-spin interaction terms with spin matrices
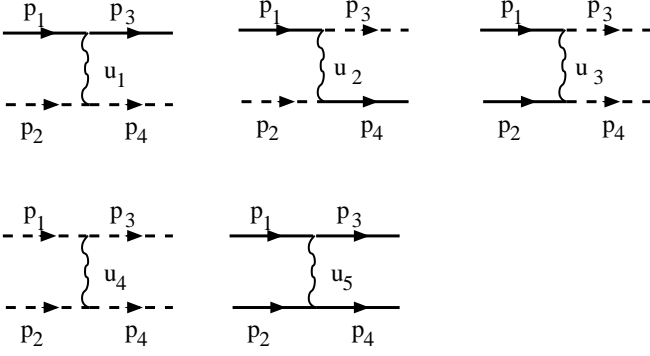
FIG. 3: Five different interactions between low-energy fermions. Solid and dashed lines represent fermions from $c-$band (near $\mathbf{k} = 0$) and $f-$band (near $\mathbf{k} = \mathbf{Q} = (\pi, \pi)$). (From Ref.[31].)

in the vertices are also possible in principle, but at weak coupling such terms are generally smaller than density-density interactions. Spin vertices, however, appear once the interactions get dressed up by singular particle-hole bubbles (see below).

III. RENORMALIZATION GROUP ANALYSIS

Interactions between low-energy fermions may generally give rise to density-wave and pairing instabilities of a Fermi liquid. These instabilities can be handled within weak-coupling theories only if the corresponding response functions are strongly enhanced, and the enhancements overcome the smallness of the interactions. One example of such behavior is a pairing instability for which one only needs an attraction in the corresponding pairing channel – a well known fact is that an arbitrary small attraction already makes the system unstable against pairing. Mathematically, this is due to the fact that at $T = 0$, particle-particle polarization bubble $\Pi_{pp}(q, \Omega)$ made out of two $c-$ fermions or out of two $f-$fermions diverges logarithmically when $q, \Omega \to 0$:

$$\Pi_{pp}^{cc}(q, \Omega) = \int \frac{d\omega d^2k}{(2\pi)^3} G_0^c(k, \omega) G_0^c(-k+q, -\omega+\Omega)$$

$$= \Pi_{pp}^{ff}(q, \Omega) = \int \frac{d\omega d^2k}{(2\pi)^3} G_0^f(k, \omega) G_0^f(-k+q, -\omega+\Omega)$$

$$= N_0 \log \frac{\Lambda}{\mathrm{max}\ (\Omega, v_F q)} \tag{4}$$

where $G_0^{c,f}(k, \omega) = (i\omega - \epsilon_k^{c,f})^{-1}$, is a free-fermion propagator and Λ is the upper cutoff.

Density-wave instabilities generally require u_i to be above a threshold of order one and are not captured within weak-coupling theory. Pnictides are special in this regard because of the nesting. The nesting implies that a particle-hole polarization bubble $\Pi_{ph}^{cf}(q+\mathbf{Q}, \Omega)$ with momentum transfer near $\mathbf{Q}$, made out of one $c-$fermion and

one $f-$fermion, also diverges logarithmically at $q, \Omega \to 0$:

$$\Pi_{ph}^{cf}(q + \mathbf{Q}, \Omega) = \int \frac{d\omega d^2k}{(2\pi)^3} G_0^c(k, \omega) G_0^f(k+q+\mathbf{Q}, \omega+\Omega)$$

$$= -N_0 \log \frac{\Lambda}{\mathrm{max}\ (\Omega, v_F q)} \tag{5}$$

Particle-hole bubbles determine the responses of a system to density-wave perturbations in spin and charge channels, and the divergence of $\Pi_{ph}^{cf}(\mathbf{Q}, 0)$ implies that the system becomes unstable towards a particular density-wave order already at a weak coupling, once the interaction in the corresponding channel becomes attractive. If there is more than one channel with attractive interaction, the order first appears in a channel where the attraction is the strongest.

The obvious issue then is what are the values of the interactions in different channels. In a generic weakly coupled Fermi liquid, the interactions are the combinations of the parameters of the Hamiltonian. Pnictides, however, are again special because, as we said, E_F is much smaller than the bandwidth W. We will see that a conventional weak-coupling behavior, in which different channels compete, only holds at $E < E_F$. At larger energies $E_F < E < W$ the system flows towards a novel fixed point at which all five interactions tend to infinity, but their ratios tend to universal values. We will see below that at this point, the symmetry extends to $SO(6)$ (Ref.[65]), and the pairing channel, the SDW channel, and also the orbital charge density-wave (CDW) channel become completely equivalent and critical.

Such symmetry, however, is only present right at the fixed point, where all five renormalized couplings are infinite, i.e., the system is on the verge of an instability. The issue then is whether the fixed point behavior is actually reached already above E_F. This depends on initial conditions.

If the fixed point is reached at some $E > E_F$, then the instability of a Fermi liquid is determined by an $SO(6)$ fixed point, and the spin and the charge density-wave orders and the pairing order emerge simultaneously, as the components of a six-dimensional order parameter. In this situation normal state Fermi liquid behavior does not exist at energies smaller than E_F. Furthermore, deviations from a perfect nesting should not change the system behavior as long as such deviations do not affect energies above E_F. If the fixed point is not reached at $E > E_F$, then the system flow at $E_F < E < W$ sets the values of the renormalized, but still finite couplings at $E \sim E_F$. These renormalized couplings then act as the "bare" couplings for the theory at energies $E < E_F$, at which spin density-wave, charge density-wave and superconductivity become competing orders, each develops at its own energy below E_F. Deviations from a perfect nesting are obviously more relevant in this situation as smaller energies are involved.

In the pnictides, both magnetic T_N and superconducting T_c are substantially smaller than $E_F \sim 1000K$, so

very likely density-wave and pairing instabilities emerge from energies below E_F, where $SO(6)$ symmetry is broken. Below we assume that this is the case and consider separately the flow of the couplings above E_F and below E_F.

A. Energies larger than E_F

In a generic weak-coupling case $u_i^{(0)} < 1$, integrating out fermions with energies between E_F and W does not substantially affect the system because the corrections to the couplings contain higher powers of $u_i^{(0)}$. However, in a situation when $E_F << W$ such renormalizations contain $u_i^{(0)} \log W/E$, where E is a running scale between E_F and W. As a result, interactions flow logarithmically from their bare values at energies of order W to their renormalized values at a scale E. When $u_i^{(0)} \log W/E$ become of order one, the renormalized couplings may differ substantially from the parameters of the Hamiltonian. Without nesting, such logarithmic renormalization would only occur in the particle-particle channel. When nesting is present, the renormalizations in both particle-particle and particle hole channels are logarithmic.

We emphasize that, at energies larger than E_F, the renormalization of the vertices from Eq. (2) is independent on what their total and transferred momenta are compared to k_F, e.g., a particle-particle vertex with *any* total momentum $k \leq k_F$ of two $c-$ or two $f-$fermions undergoes the same renormalization. Similarly, vertices with transferred momenta between $c-$and $f-$fermions $k' = \mathbf{Q} + q$ undergo the same renormalization for all $q \sim k_F$.

As it is customary to weak coupling theories, below we only consider renormalizations which contain powers of $u_i^{(0)} \log W/E$ and neglect regular renormalizations which bring additional powers of $u_i^{(0)}$. In a diagrammatic language, this amounts to summing up series of diagrams and keeping the highest power of the logarithm at every order. The presence of two orthogonal channels of logarithmic renormalizations implies that one needs to sum up parquet series of diagrams (see, e.g. Ref.[66]). We explicitly verified, by evaluating diagrams up to third order in $u_i^{(0)}$, that the system is renormalizable, i.e., that, instead of summing up infinite series of diagrams, one can write up one-loop parquet RG equations. The derivation of the RG equations is straightforward (see Fig. 4). Evaluating second-order diagrams and collecting combinatoric pre-factors, we obtain the set of equations

$$\dot{u}_1 = u_1^2 + u_3^2$$
$$\dot{u}_2 = 2u_2(u_1 - u_2)$$
$$\dot{u}_3 = u_3(4u_1 - 2u_2 - u_4 - u_5)$$
$$\dot{u}_4 = -u_3^2 - u_4^2$$
$$\dot{u}_5 = -u_3^2 - u_5^2, \tag{6}$$

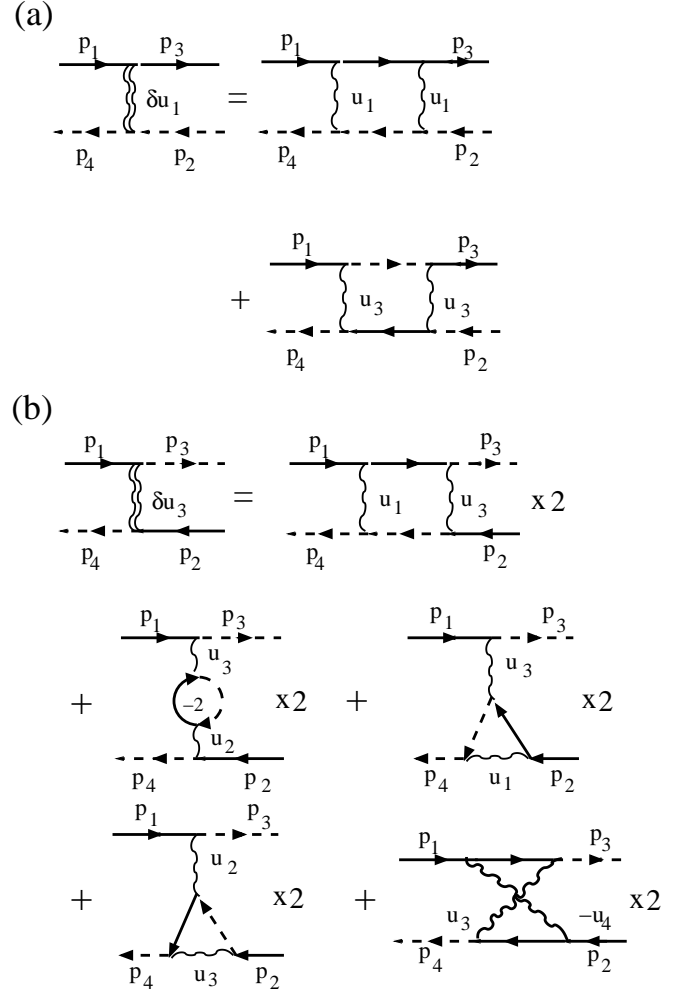where the derivatives are with respect to $L =$

(a)

(b)

FIG. 4: Diagrams for the one-loop vertex renormalizations. The diagrams for the renormalizations of u_1 and u_3 terms are shown. The diagrams for the renormalization of u_2, u_4, and u_5 terms are obtained in a similar fashion. (From Ref.[31].)

$(1/2) \log W/E$. The factor $1/2$ reflects the fact that each of the fermionic bands extends to energies above E_F only in one direction. This factor was neglected in Ref.[31]. Similar, though not identical equations have been obtained in the weak-coupling analysis of the cuprates for "$t-$only" dispersion[66].

The RG equations for the couplings u_4 and u_5 are identical and preserve particle-hole symmetry. Below we only use u_4. Note that all couplings remain momentum-independent under one-loop RG. The momentum dependence appears beyond the leading logarithmic approximation, and is small at weak coupling.

We see from Eq.(6) that the pair hopping term u_3 is not generated by other interactions, *i.e.*, $u_3 = 0$ if $u_3^{(0)} = 0$. When $u_3^{(0)} = 0$, the set (6) decouples into

$$\dot{u}_1 = u_1^2$$
$$(2\dot{u}_2 - \dot{u}_1) = -(2u_2 - u_1)^2$$
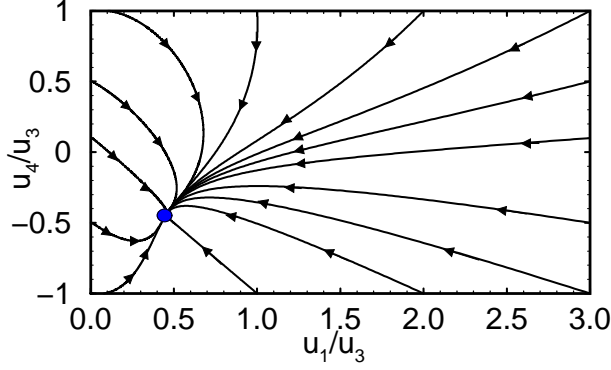$$\dot{u}_4 = -u_4^2 \tag{7}$$

FIG. 5: (color online) The RG flow of Eqn. (6) in variables u_4/u_3 and u_1/u_3 (from Ref.[31]). The fixed point is $u_4/u_3 = -1/\sqrt{5}$, $u_1/u_3 = 1/\sqrt{5}$. For definiteness, we used boundary conditions $u_1^{(0)} = u_4^{(0)}$, $u_3^{(0)} = 0.1u_1^{(0)}$, and set $u_0^2 = 0$. (From Ref.[31].)

In this special case, particle-hole and particle-particle channels decouple: $u_4 = u_4^{(0)}/(1 + 0.5u_4^{(0)} \log W/E)$ is renormalized in the particle-hole channel and flows to zero for $u_4^{(0)} > 0$. [By the same reason, strong Coulomb repulsion renormalizes down at low energies in conventional SC and allows electron-phonon interaction to overcome it at small frequencies[67]]. The renormalization of the inter-pocket interaction u_1 comes from particle-hole channel, is of opposite sign, and $u_1 = u_1^{(0)}/(1 - 0.5u_1^{(0)} \log W/E)$ increases when E decreases. The renormalization of $2u_2 - u_1$ also comes from particle-hole channel, and u_2 tends to $u_1/2$ when $2u_2^{(0)} - u_1^{(0)} > 0$.

Once $u_3^{(0)}$ is finite, the system moves into the basin of attraction of another fixed point at which all couplings simultaneously tend to infinity and u_3 becomes the largest. Indeed, introducing $u_2 = \alpha u_1$, $u_3 = \beta u_1$, and $u_4 = \gamma u_1$, we can re-write Eq. (6) as

$$\dot{u}_1 = u_1^2(1 + \beta^2),$$
$$\dot{\alpha} = u_1\alpha \left(1 - 2\alpha - \beta^2\right),$$
$$\dot{\beta} = u_1\beta \left(3 - 2(\alpha + \gamma) - \beta^2\right),$$
$$\dot{\gamma} = -u_1(1 + \gamma) \left(\beta^2 + \gamma\right).$$
$$(8)$$

The new fixed point corresponds to $\dot{\alpha} = \dot{\beta} = \dot{\gamma} = 0$, i.e., to

$$\alpha \left(1 - 2\alpha - \beta^2\right) = 0,$$
$$\beta \left(3 - 2(\alpha + \gamma) - \beta^2\right) = 0,$$
$$(1 + \gamma) \left(\beta^2 + \gamma\right) = 0.$$
$$(9)$$

For $\beta \neq 0$ (i.e., $u_3 \neq 0$), the solution of the set is $\alpha = 0$, $\gamma = -1$, $\beta = \pm\sqrt{5}$. There are no other solutions for

$\beta \neq 0$. Expanding near this fixed point we obtain

$$\dot{u}_1 \approx 6u_1^2, \quad \dot{\alpha} = -4u_1 \, \alpha,$$
$$\dot{x} \approx 5x \, u_1 \, (2\alpha + 2z + x), \quad \dot{z} = -4u_1 \, z. \quad (10)$$

where $z = 1 + \gamma$ and $x = \beta^2 - 5$. Solving this set, we find that u_1 increases, while α, x and z all scale as $u_1^{-2/3}$ and vanish when u_1 diverges. This implies that the fixed point specified by (9) is a stable fixed point.

We see that $|u_3|$ becomes the largest coupling at the fixed point, while $u_4 = -u_1$, and $u_1 = |u_3|/\sqrt{5}$. The sign of u_3 at the fixed point is the same as the sign of $u_3^{(0)}$, i.e., it is positive for $u_3^{(0)} > 0$ and negative for $u_3^{(0)} < 0$. Using $\alpha \propto u_1^{-2/3}$, we find that near a fixed point $u_2 \propto |u_3|^{1/3}$. We also verified that a fixed point with $u_3 = 0$ (i.e., $\beta = 0$) is an unstable fixed point, while the one for which u_3 is the largest coupling is a stable fixed point.

In Fig.5 we show the RG flow obtained by a numerical solution of Eq. (6). We see that the system indeed flows towards a stable fixed point for any $u_3^{(0)} \neq 0$. On the other hand, this stable fixed point is reached only at an infinite coupling. As long as u_i are finite, the system flows towards the stable fixed point, but does not reach it. A scale when u_i diverge is $\log W/E < 1/u^*$, where u^* is some linear combination of the bare u_i^0. Like we said, we assume that at $E = E_F$, the couplings are still finite, i.e., this fixed point is not yet reached. In practical terms, this implies that $\log W/E_F < 1/u^*$.

How the system flows depends on the values and signs of the bare u_i. We assume that all bare interactions are repulsive, $u_i > 0$. Then, under RG flow, u_1 and u_3 increase, while u_4 decreases, passes through zero, *changes sign*, becomes negative and approaches $-u_1$. The coupling u_2 also increases, but becomes relatively small compared to other couplings. The sign change of u_4 is the consequence of the coupling between particle-hole and particle-particle channels. If particle-hole channel was not logarithmic, the RG equation for u_3 would reduce to $\dot{u}_3 = -2u_3u_4$. Solving this equation together with the equation for u_4 one would obtain that, for $u_4^{(0)} > |u_3^{(0)}|$, the intra-pocket repulsion u_4 would preserve its sign and just decrease logarithmically under RG together with the pair-hopping term.

B. Energies smaller than E_F

The RG flow described by Eqs (6) stops at $E \sim E_F$. At smaller energies the independence of the RG equations of the total and transferred momenta is lost, and, e.g., the vertex u_3 with zero total momentum of two $c-$fermions is renormalized differently from the same vertex with the total momentum of order k_F. To put it simply, only two types of vertices continue to flow logarithmically at energies below E_F – the vertices with zero total momentum of two $c-$ or two $f-$fermions, and (for the case of a perfect nesting) the vertices with the momentum transfer

between c and $f-$fermions exactly equal to $\mathbf{Q}$. The vertices with zero total momentum are u_4 and u_3 terms, the vertices with the momentum transfer $\mathbf{Q}$ are u_1, u_2 ,and u_3 terms. The vertex u_3 with zero total momentum generally has an arbitrary momentum transfer $\mathbf{Q} + q$, where $q \sim k_F$. The vertex u_3 with the momentum transfer $\mathbf{Q}$ has the total incoming momentum of order k_F. For all other vertices, the RG flow is cut at E_F.

We will use the values of u_i at E_F as the "bare" couplings for the theory at $E < E_F$ and label them as $\bar{u}_i$ ($\bar{u}_i = u_i(E = E_F)$). The upper limit for the RG at $E < E_F$ is then obviously E_F. We label the couplings with zero total momentum as $u_3(0)$ and $u_4(0)$ and the couplings with momentum transfer $\mathbf{Q}$ as $u_1(Q)$, $u_2(Q)$, and $u_{3a}(Q)$, and $u_{3b}(Q)$. The separation into u_{3a} and u_{3b} is due to the fact that there are two different u_3 vertices with momentum transfer $\mathbf{Q}$: the coupling u_{3a} corresponds to $p_3 = p_1 + \mathbf{Q}$ in the u_3 vertex in Fig. 3, while u_{3b} corresponds to $p_1 = p_4 + \mathbf{Q}$.

The RG equations for the relevant couplings are obtained in the same way as at higher energies, but now one has to carefully analyze which diagrams still yield $\log E_F/E$ and in which diagrams the logarithm is cut. For example, the renormalization of $u_3(0)$ comes from the first diagram in Fig. (4), the renormalization of $u_{3a}(Q)$ comes from the second, third, and fourth diagrams, and the renormalization of $u_{3b}(Q)$ comes only from the third diagram. Evaluating the diagrams, we obtain

$$\frac{du_1(Q)}{dL} = u_1^2(Q) + u_{3b}^2(Q), \quad \frac{du_{3b}(Q)}{dL} = 2u_{3b}(Q)u_1(Q),$$
$$\frac{du_2(Q)}{dL} = 2u_2(Q)(u_1(Q) - u_2(Q)) + 2u_{3a}(Q)(u_{3b}(Q) - u_{3a}(Q)),$$
$$\frac{du_{3a}(Q)}{dL} = -4u_{3a}(Q)u_2(Q)) + 2u_2(Q)u_{3b}(Q) + 2u_{3a}(Q)u_1(Q),$$
$$\frac{du_3(0)}{dL} = -2u_3(0)u_4(0), \quad \frac{du_4(0)}{dL} = -u_3^2(0) - u_4^2(0).$$

$$(11)$$

where now $L = \log E_F/E$. From (11) we immediately obtain

$$\frac{d}{dL} \left(u_1(Q) + u_{3b}(Q) \right) = (u_1(Q) + u_{3b}(Q))^2, \quad \frac{d}{dL} \left(u_{3b}(Q) - u_1(Q) \right) = -(u_{3b}(Q) - u_1(Q))^2,$$
$$\frac{d}{dL} \left(u_1(Q) + u_{3b}(Q) - 2(u_2(Q) + u_{3a}(Q)) \right) = (u_1(Q) + u_{3b}(Q) - 2(u_2(Q) + u_{3a}(Q)))^2,$$
$$\frac{d}{dL} \left(u_1(Q) - u_{3b}(Q) - 2(u_2(Q) - u_{3a}(Q)) \right) = (u_1(Q) - u_{3b}(Q) - 2(u_2(Q) - u_{3a}(Q)))^2,$$
$$\frac{d}{dL} \left(u_3(0) - u_4(0) \right) = (u_3(0) - u_4(0))^2, \quad \frac{d}{dL} \left(u_3(0) + u_4(0) \right) = -(u_3(0) + u_4(0))^2.$$

$$(12)$$

These equations can be easily solved and yield

$$u_1(Q) + u_{3b}(Q) = \frac{\bar{u}_1 + \bar{u}_3}{1 - (\bar{u}_1 + \bar{u}_3) \log \frac{E_F}{E}}, \quad u_1(Q) - u_{3b}(Q) = \frac{\bar{u}_1 - \bar{u}_3}{1 - (\bar{u}_1 - \bar{u}_3) \log \frac{E_F}{E}},$$
$$u_1(Q) + u_{3b}(Q) - 2(u_2(Q) + u_{3a}(Q)) = \frac{\bar{u}_1 - \bar{u}_3 - 2\bar{u}_2}{1 - (\bar{u}_1 - \bar{u}_3 - 2\bar{u}_2) \log \frac{E_F}{E}},$$
$$u_1(Q) - u_{3b}(Q) - 2(u_2(Q) - u_{3a}(Q)) = \frac{\bar{u}_1 + \bar{u}_3 - 2\bar{u}_2}{1 - (\bar{u}_1 + \bar{u}_3 - 2\bar{u}_2) \log \frac{E_F}{E}},$$
$$u_3(0) - u_4(0) = \frac{\bar{u}_3 - \bar{u}_4}{1 - (\bar{u}_3 - \bar{u}_4) \log \frac{E_F}{E}}, \quad u_3(0) + u_4(0) = \frac{\bar{u}_3 + \bar{u}_4}{1 + (\bar{u}_3 + \bar{u}_4) \log \frac{E_F}{E}}.$$

$$(13)$$

We see that there are six different energies E at which different combinations of the couplings diverge or may diverge

IV. DENSITY-WAVE AND PAIRING INSTABILITIES

We now relate the divergences of these six combinations of the couplings with density-wave and pairing in-

stabilities for our model. We searched for SDW and CDW instabilities with momentum $\mathbf{Q}$ and with either real or imaginary order parameter, and for a SC instability either in pure s channel (the gaps Δ_c and Δ_f have the same sign), or in s^+ channel (the gaps Δ_c and Δ_f have opposite sign). The instabilities with momentum-dependent order parameter, like a nematic instability[61] or a $d-$wave superconductivity[37,38] do not occur in our model because we set bare interactions to be momentum-independent and considered only the leading logarith-
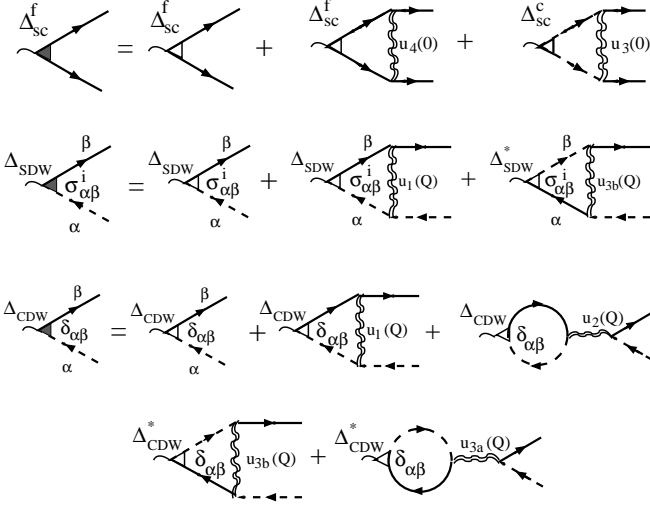
FIG. 6: Diagrammatic representation of the renormalized vertices in SDW, CDW, and SC channels. The shaded triangles are fully renormalized vertices, double lines represent running couplings given by Eq. (13).

mic renormalizations of the vertices. The momentum dependence of the vertices comes from subleading, non-logarithmic renormalizations which we neglected.

Density-wave and pairing susceptibilities are obtained by standard means: by introducing an infinitesimal coupling in a particular channel and evaluating the response. For this, we add to the Hamiltonian three extra terms

$$
\Delta_{sdw} \sum_k c^\dagger_{\mathbf{k},\alpha} \sigma^z_{\alpha\beta} f_{\mathbf{k+Q},\beta},
$$
$$
\Delta_{cdw} \sum_k c^\dagger_{\mathbf{k},\alpha} \delta_{\alpha\beta} f_{\mathbf{k+Q},\beta},
$$
$$
\Delta^c_{sc} \sum_k c_{\mathbf{k},\alpha} \sigma^y_{\alpha\beta} c_{-\mathbf{k},\beta} + \Delta^f_{sc} \sum_k f_{\mathbf{k+Q},\alpha} \sigma^y_{\alpha\beta} f_{-\mathbf{k-Q},\beta}
$$
$$(14)$$

with complex Δ_{sdw}, Δ_{cdw}, and real $\Delta^{c,f}_{sc}$, and evaluate how these terms are renormalized by u_i. The corresponding diagrams are presented in Fig. 6. In analytic form, the fully renormalized vertices at an energy E (or, equivalently, at a temperature T) are given by

$$
\Delta^{full}_j = \Delta_j \left(1 + \Gamma_j \log \frac{E_F}{E} \right) \tag{15}
$$

where j corresponds to either SC, or SDW, or CDW order parameters. We label corresponding Γ_j as $\Gamma^{(r,i)}_{SDW}$, $\Gamma^{(r,i)}_{CDW}$, and $\Gamma^{(s,s^+)}_{SC}$, where r,i mean real or imaginary density-wave order, and s, s^+ mean $s-$wave or extended $s-$wave SC order, respectively. An instability towards a particular SDW, CDW or SC order occurs at a temperature $T^{r,i}_{SDW}$, $T^{r,i}_{CDW}$, or T^{s,s^+}_{SC}, at which the corresponding $\Gamma_j(E)$ diverges.
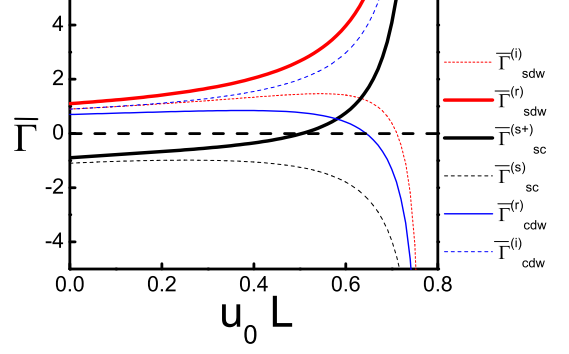

FIG. 7: (color online) The values of effective interactions $\bar{\Gamma}_j$ in various density-wave and superconducting channels at an energy $E \sim E_F$ vs $L = \log W/E_F$. The effective interactions are linear combinations of $\bar{u}_i$ (Eq. (18)), which are the solutions of the RG set (6). For definiteness we set bare parameters $u_1^{(0)} = u_4^{(0)} = u_0$, and $u_2^{(0)} = u^{(0)}_3 = 0.1u_0$. All $\bar{\Gamma}_j$ are in units of u_0. Observe that the strongest interaction is in SDW channel, and that $\bar{\Gamma}^{s^+}_{SC}$ changes sign and becomes attractive once L exceeds some critical value. (From Ref.[31] with permission from the authors.)

From Fig. 6, we have

$$
\Gamma^{(r)}_{SDW} = u_1(Q) + u_{3b}(Q), \quad \Gamma^{(i)}_{SDW} = u_1(Q) - u_{3b}(Q),
$$
$$
\Gamma^{(r)}_{CDW} = u_1(Q) + u_{3b}(Q) - 2(u_2(Q) + u_{3a}(Q)),
$$
$$
\Gamma^{(i)}_{CDW} = u_1(Q) - u_{3b}(Q) - 2(u_2(Q) - u_{3a}(Q)),
$$
$$
\Gamma^{(s)}_{SC} = -(u_4(0) + u_3(0)), \quad \Gamma^{(s^+)}_{SC} = u_3(0) - u_4(0) \tag{16}
$$

We see that these vertices contain exactly the same six combinations of parameters which we analyzed in the previous section. Combining Eqs. (12), (13) and (16) we find that all six channels are *decoupled* at energies below E_F, all Γ_j satisfy the same RG equation

$$
\frac{d\Gamma_j}{dL} = \Gamma_j^2 \tag{17}
$$

The interplay between different instabilities is then determined by the bare values of Γ_j in different channels, which are $\Gamma_j(E \sim E_F)$. This implies that SDW, CDW, and SC orders are *competing orders* in this approximation. The first instability occurs in the channel for which the coupling at $E \sim E_F$ is the largest.

At $E \sim E_F$, $u_i = \bar{u}_i$, and we have ($\Gamma_j(E \sim E_F) = \bar{\Gamma}_j$)

$$
\bar{\Gamma}^{(r)}_{SDW} = \bar{u}_1 + \bar{u}_3, \quad \bar{\Gamma}^{(i)}_{SDW} = \bar{u}_1 - \bar{u}_3,
$$
$$
\bar{\Gamma}^{(r)}_{CDW} = \bar{u}_1 - \bar{u}_3 - 2\bar{u}_2, \quad \bar{\Gamma}^{(i)}_{CDW} = \bar{u}_1 + \bar{u}_3 - 2u_2,
$$
$$
\bar{\Gamma}^{(s)}_{SC} = \bar{u}_4 + \bar{u}_3, \quad \bar{\Gamma}^{(s^+)}_{SC} = \bar{u}_4 - \bar{u}_3 \tag{18}
$$

We see that Γ^r_{SDW} diverges when

$$
\log \frac{E_F}{E} = \frac{1}{\bar{\Gamma}^r_{SDW}} = \frac{1}{\bar{u}_3 + \bar{u}_1} \tag{19}
$$

if $\bar{u}_3 + \bar{u}_1 > 0$. The vertex Γ^i_{SDW} diverges at

$$\log \frac{E_F}{E} = \frac{1}{\bar{\Gamma}^i_{SDW}} = \frac{1}{\bar{u}_1 - \bar{u}_3} \tag{20}$$

if $\bar{u}_1 > \bar{u}_3$. The vertex Γ^i_{CDW} diverges at

$$\log \frac{E_F}{E} = \frac{1}{\bar{\Gamma}^i_{CDW}} = \frac{1}{\bar{u}_1 + \bar{u}_3 - 2\bar{u}_2} \tag{21}$$

if $\bar{u}_1 + \bar{u}_3 - 2\bar{u}_2 > 0$. The vertex Γ^r_{CDW} diverges at

$$\log \frac{E_F}{E} = \frac{1}{\bar{\Gamma}^r_{CDW}} = \frac{1}{\bar{u}_1 - \bar{u}_2 - 2\bar{u}_2} \tag{22}$$

if $\bar{u}_1 - \bar{u}_3 - 2\bar{u}_2 > 0$. The vertex Γ^s_{SC} diverges when

$$\log \frac{E_F}{E} = \frac{1}{\bar{\Gamma}^s_{SC}} = \frac{-1}{\bar{u}_3 + \bar{u}_4} \tag{23}$$

if $\bar{u}_3 + \bar{u}_4 < 0$. The vertex $\Gamma^{s^+}_{SC}$ diverges when

$$\log \frac{E_F}{E} = \frac{1}{\bar{\Gamma}^{s^+}_{SC}} = \frac{1}{\bar{u}_3 - \bar{u}_4} \tag{24}$$

if $\bar{u}_3 > \bar{u}_4$.

Strictly speaking, only the largest E (for which $\log E_F/E$ is the smallest) has physical meaning within this approach as a Fermi liquid does not exist below this energy. However, when two or more critical E are close, the system may have a sequence of phase transitions.

In Fig. 7 we show how these $\bar{\Gamma}_j$ evolve depending on the value of $L = \log W/E_F$. We see that for our choice of $u_i^0 > 0$ $\bar{\Gamma}^r_{SDW}$ is the largest, and the highest critical E is when Γ^r_{SDW} diverges. This implies that for a perfect nesting the first instability of a normal state occurs in the SDW channel and leads to a real SDW order parameter. This happens at

$$T^r_{SDW} \propto \exp\left[-\frac{1}{\bar{u}_1 + \bar{u}_3}\right] \tag{25}$$

At the same time, the energies at which Γ^i_{CDW} and $\Gamma^{s^+}_{SC}$ diverge are only slightly smaller if the bare couplings $\bar{u}_i$ are close to their fixed point values $\bar{u}_3 = \sqrt{5}\bar{u}_1$, $\bar{u}_4 = -\bar{u}_1$, $\bar{u}_2 << \bar{u}_1$: instability towards CDW order with an imaginary order parameter (an orbital order) occurs at

$$T^i_{CDW} \propto \exp\left[-\frac{1}{\bar{u}_1 + \bar{u}_3 - 2\bar{u}_2}\right] \tag{26}$$

and the instability in the s^+ SC channel occurs at

$$T^{s^+}_{SC} \propto \exp\left[-\frac{1}{\bar{u}_3 - \bar{u}_4}\right] \tag{27}$$

Whether CDW and SC orders emerge as additional orders at a smaller T requires a separate analysis as density-wave and the pairing susceptibilities change in the presence of an SDW order. Ref. [40] found that additional orders do not occur for a perfect nesting.

We emphasize again the the special role of the RG renormalization at energies higher than E_F. The bare couplings $u_3^{(0)}$ and $u_4^{(0)}$ are the parameters of the Hamiltonian, and without RG flow at intermediate energies, there would be no divergence of the couplings at zero total momentum if $u_4^{(0)} > u_3^{(0)}$. Moreover, it is very likely that in pnictides $u_4^{(0)}$ is larger than $u_3^{(0)}$ because $u_4^{(0)}$ comes from the Hubbard repulsion within a given orbital, while $u_3^{(0)}$ comes from inter-orbital processes which is generally though to be weaker[37,44,68]. However, we know that the renormalization from energies above E_F strongly affects u_4 and not only reduces its magnitude but forces it to change sign and become negative. In this situation, at energies of order E_F, $\bar{u}_3 - \bar{u}_4 > 0$ even if $u_3^{(0)} - u_4^{(0)} < 0$, and the fully renormalized $u_3(0) - u_4(0)$ diverges at E given by (24).

When nesting becomes non-perfect (e.g. upon doping), the interplay between different instabilities changes. The pairing channel still remains logarithmic, and $T^{s^+}_{SC}$ is given by (27). In the density-wave channels, the polarization bubble made of $c-$and $f-$fermions with momentum transfer $\mathbf{Q}$ remains logarithmic ($\log E_F/E$) only for E larger than the energy scale δ associated with non-nesting. At smaller energies, the logarithm is cut. Accordingly, $T^r_{SDW}(\delta)$ and $T^i_{CDW}(\delta)$ decrease, and at some deviation from a perfect nesting, $T^r_{SDW}(\delta) = T^{s^+}_{SC}$. At larger δ, the first instability of a Fermi-liquid is into a SC state with an s^+ symmetry of a superconducting gap.

The actual transformation from an SDW to a SC state is more involved because SDW state for a non-perfect doping eventually becomes incommensurate[35,40], like in chromium[32,33]. The incommensurate state is a magnetic analog of the Fulde-Ferrell-Larkin-Ovchinnikov (FFLO) state[69] of a superconductor in a magnetic field[32,35]. Depending on whether or not a SDW order becomes incommensurate before superconductivity emerges, the transition from a SDW antiferromagnet to a s^+ SC is either first order or involves an intermediate phase in which SC order co-exists with an incommensurate SDW order[40] (see Fig. 8). A peak in the spin susceptibility at an incommensurate momentum near $\mathbf{Q}$. has been observed in the weak-coupling, RPA analysis of a multi-orbital Hubbard-like model[37] (five Fe bands). This and other studies[38,39] also reported smaller peaks in the susceptibility at a smaller momenta, possibly related to $2k_F$.

A. $SO(6)$ symmetry

For completeness, we also consider a situation when hole and electron pockets are so small in size that the regime $W > E > E_F$ extends down to an energy at which u_i diverge, and the ratios of the couplings approach their fixed point values $u_3/u_1 = \sqrt{5}$, $u_4 = -u_1$ and $u_2/u_1 \to 0$. In this situation, the system becomes unstable even before it enters a regime $E < E_F$. One can immediately see from (16) that in this situation $\Gamma^r_{SDW} = \Gamma^i_{CDW} =$

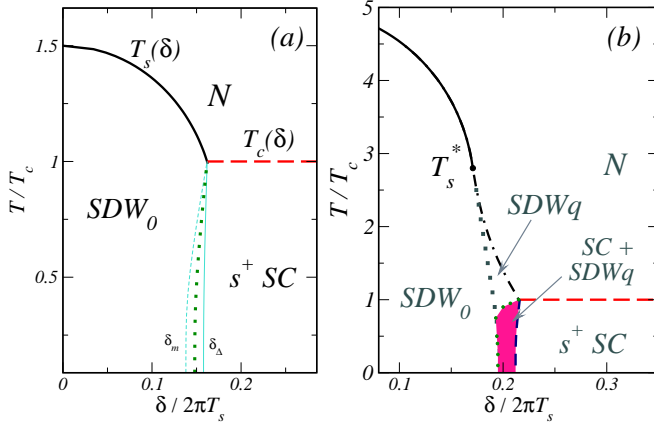FIG. 8: (color online) Phase diagram for $T_s/T_c = 1.5$ (a) and $T_s/T_c = 5$ (b), where $T_s = T^r_{sdw}$ and $T_c = T^{s+}_{SC}$. δ measures a deviation from a perfect nesting in energy units (from Ref.[40]). On the left panel thick solid and dashed lines represent second-order SDW and SC transitions, dotted line represents first order transition between commensurate SDW (SDW$_0$) and s^+ SC states, and light lines denoted by δ_Δ and δ_m are instability lines of SC and SDW phases, surrounding a first-order transition line. On the right panel, an incommensurate SDW order appears below $T_s(\delta)$ once it becomes smaller than $T^*_s = 0.56T_s > T_c$. Below T_c, a new mixed phase appears in which incommensurate SDW$_q$ order co-exists with SC. At small T, there is no SDW$_q$ state without superconductivity. The transitions into the mixed state are second order from a SC state and first order from a commensurate SDW state. The transition from the normal state (N) to SDW$_q$ state is second order (dashed-dotted line), and from SDW$_q$ to SDW$_0$ is first order (dotted line). (From Ref.[40] with permission from the authors.)

Γ^{s+}_{SC}, i.e., SDW order, orbital CDW order, and s^+ SC order appear simultaneously.

The system behavior at such critical point has been discussed in detail by Podolsky, Kee, and Kim[65]. They demonstrated that the fixed point Hamiltonian has $SO(6)$ symmetry, and found 15 operators which form the Lie algebra of the $SO(6)$ group. They found that the three interaction channels are indeed equivalent, and the order parameter is a six-component vector. Two components are the pairing amplitude and the phase, three components are spin projections, and the remaining component is an imaginary charge order parameter. The direction of this six-component vector is not specified by the Hamiltonian and set up by by a spontaneous breaking of the $SO(6)$ symmetry. An even larger symmetry is expected once one takes into consideration the fact that there are two hole and two electron FS[70]

In pnictides, the temperatures of magnetic and superconducting instabilities are 10-20 times smaller than E_F, and it is therefore unlikely that the normal state becomes unstable already at $E > E_F$, although to firmly establish this would require more involved calculations than the weak-coupling analysis which we present here. At the same time, even approximate $SO(6)$ symmetry should

affect system properties at intermediate energies. For example, a dispersing magnetic resonance mode in an s^+ superconducting state has a velocity $v = v_F/\sqrt{2}$ (Ref.[31]), the same as the velocity of the Anderson-Bogolubov phase mode in a 2D uncharged superconductor. A number of collective properties associated with an approximate $SO(6)$ symmetry were considered in [65].

V. IS THE PAIRING MAGNETICALLY MEDIATED?

In this section we consider in more detail the case when an instability of a normal state occurs well below E_F. We found earlier that the flow towards $SO(6)$ fixed point is cut at E_F, and at smaller energies SC, SDW, and CDW channels decouple, i.e., SC, SDW, and CDW become competing orders. Each develops independently, and the one with the highest instability temperature wins.

This is true however only in the leading logarithmic approximation. Beyond it, there is still a residual coupling between SC and density-wave channels, and the issue is whether this residual coupling may lead to a new physics. In particular, near a SDW instability, magnetic susceptibility near $\mathbf{Q}$ is strongly enhanced. If there is a residual coupling between SC and SDW channels, the pairing interaction should generally have a component which can be viewed as the exchange of antiferromagnetic spin fluctuations. At weak coupling, this component has an extra smallness simply because it comes from residual interaction, but this smallness may be compensated by the enhancement of the antiferromagnetic spin susceptibility $\chi_s(\mathbf{Q})$. If the enhancement of $\chi_s(\mathbf{Q})$ wins over the overall smallness of the residual interaction, spin fluctuation exchange becomes the dominant component of the pairing interaction.

The idea that the pairing near a magnetic instability is mediated by spin fluctuations has been applied to various systems, most notably to the cuprates[71], where this mechanism of electronic pairing unambiguously yields $d_{x^2-y^2}$ symmetry of the pairing gap. In the cuprates, however, there is only one large hole FS in the normal (not pseudogap) state, and the couplings are by no means small.

Below we first derive the effective interaction and show that it indeed contains an extra term with the spin-fluctuation exchange. We then estimate the relative strength of this term compared to a direct u_3-u_4 pairing interaction which we obtained earlier.

For $u_i^{(0)} << 1$, the residual coupling between SDW and SC channels can be actually obtained in a controlled way. The term which contributes to both SC and SDW is the pair-hopping u_3 term. Earlier in the paper we separated this term into $u_3(0)$, which is the interaction with zero total momentum: $u_3(0) = u_3(k,-k;p+Q,-p-Q)$, and $u_{3a}(Q)$ and $u_{3b}(Q)$ which are two interactions with momentum transfer $\mathbf{Q}$: $u_{3a} = u_3(k,p;k+Q,p-Q)$, and $u_{3b} = u_3(k,p,p-Q,k+Q)$. The first two momenta

are for $c-$fermions, the other two are for $f-$fermions. Like before, we shift the momenta of $f-$fermions by $\mathbf{Q}$. In these new notations, $u_3(0) = u_3(k, -k; p, -p)$, $u_{3a} = u_3(k, p; k, p)$, $u_{3b} = u_3(k, p, p, k)$. Interactions u_{3a} and u_{3b} are density-wave vertices, and $u_3(0)$ is a pairing vertex. Since both SC and SDW instabilities are confined to the FS, we restrict the interactions to $|\mathbf{k}| = |\mathbf{p}| = k_F$.

We now observe that, already at this stage, there is an overlap of measure zero between the pairing and density-wave vertices because the vertices u_{3a} and u_{3b} are defined for *any* angle between $\mathbf{k}$ and $\mathbf{p}$, including $\mathbf{p} = -\mathbf{k}$. At this particular point $u_{3a} = u_3(k, -k, ; k, -k)$ and $u_{3b} = u_3(k, -k; -k, k)$ become components of the particle-particle vertex, albeit for a single momentum transfer. One should indeed exercise care to avoid double counting of the pairing interaction. In practice, this means that one has to subtract from u_{3a} and u_{3b} their bare value $\bar{u}_3$. Still, even after this subtraction, u_{3a} and u_{3b} diverge at a SDW transition, i.e., there exists a formally divergent component of the pairing potential, although at this stage it is only present for a single momentum transfer.

The overlap of measure zero has no physical effect, but we can extend the analysis by including into the pairing vertex the terms u_{3a} and u_{3b} at zero total momentum and at small but finite momentum and frequency transfers $\mathbf{q}$, and ω. In our notations, these vertices are $u_{3a}(k, -k; k + q, -k - q)$ and $u_{3b}(k, -k, -k - q, k + q)$ $(q = (\mathbf{q}, \omega))$. These two vertices do not diverge at a SDW transition, but still are enhanced at small q. An important observation here is that these u_{3a} and u_{3b} still come from the same series of diagrams as at $q = 0$ – the only adjustment is in the argument of the logarithm. All other additions to the pairing interaction are regular functions of q and can be safely neglected because of small overall factor. In other words, a potentially relevant pairing component due to residual interaction between SDW and SC channels can be explicitly obtained from our earlier diagrammatic analysis, by extending it to a small but finite q and keeping the same diagrams. This reasoning parallels the one used in the derivation of the fully renormalized vertex functions in a Fermi liquid with predominantly forward scattering[72].

To obtain $u_{3a}(k, -k; k + q, -k - q)$ and $u_{3b}(k, -k, -k - q, k + q)$ we note that near a SDW instability, $u_1(Q) + u_{3b}(Q)$ diverge as $(\bar{u}_1 + \bar{u}_3)/(1 - (\bar{u}_1 + \bar{u}_3)L)$, while $u_1(Q) - u_3(Q)$, $u_2(Q) - u_{3a}(Q)$ and $u_1(Q) + u_{3a}(Q) - 2(u_2(Q) + u_{3b}(Q))$ remain finite. Elementary calculations then show that

$$u_{3a}(Q) \approx \frac{1}{2}u_{3b}(Q) \approx \frac{1}{4}\frac{(\bar{u}_1 + \bar{u}_3)}{1 - (\bar{u}_1 + \bar{u}_3)L} \qquad (28)$$

Extending the result to a finite q, and subtracting the bare values to avoid double counting, we obtain, in our notations

$$u_{3a}(k, -k, k + q, -k - q) = u_{3a}^{eff}(q) = \frac{1}{4}\frac{(\bar{u}_1 + \bar{u}_3)^2 L_q}{1 - (\bar{u}_1 + \bar{u}_3)L_q}$$

$$u_{3b}(k, -k, -k - q, k + q) = u_{3b}^{eff}(q) = \frac{1}{2}\frac{(\bar{u}_1 + \bar{u}_3)^2 L_q}{1 - (\bar{u}_1 + \bar{u}_3)L_q}$$
$$(29)$$

where $L_q = \log E_F/E_q$ and $E_q^2 = E^2 + av_F\mathbf{q}^2 + b\omega^2$, $a, b = O(1)$. These expressions are only valid at small q, when u_{3a}^{eff} and u_{3b}^{eff} are enhanced. Note the difference with a Cooperon in a disordered metal: there, E_q contains $|\omega|$ term[73].

Combining the two interactions given by (29) with the original bare interaction in the s^+ pairing channel $\bar{u}_3 - \bar{u}_4$ we obtain irreducible, antisymmetrized pairing vertex $\Gamma_{\alpha\beta,\gamma\delta}(k, -k, p, -p)$ in the form

$$\Gamma_{\alpha\beta,\gamma\delta}(k, -k, p, -p) = (\bar{u}_3 - \bar{u}_4)(\delta_{\alpha\beta}\delta_{\gamma\delta} - \delta_{\alpha\delta}\delta_{\beta\gamma})$$
$$+ u_{3a}^{eff}(k - p)\delta_{\alpha\beta}\delta_{\gamma\delta} - u_{3b}^{eff}(k - p)\delta_{\alpha\delta}\delta_{\beta\gamma} \qquad (30)$$

Using $\delta_{\alpha\delta}\delta_{\beta\gamma} = (\delta_{\alpha\beta}\delta_{\gamma\delta} + \vec{\sigma}_{\alpha\beta}\vec{\sigma}_{\gamma\delta})/2$ and $u_{3a}^{eff}(k - p) = 0.5u_{3b}^{eff}(k - p)$, we further obtain from (30)

$$\Gamma_{\alpha\beta,\gamma\delta}(k, -k, p, -p) = \frac{1}{2}(\bar{u}_3 - \bar{u}_4)(\delta_{\alpha\beta}\delta_{\gamma\delta} - \vec{\sigma}_{\alpha\beta}\vec{\sigma}_{\gamma\delta})$$
$$- \frac{1}{2}u_{3b}^{eff}(k - p)\vec{\sigma}_{\alpha\beta}\vec{\sigma}_{\gamma\delta} \qquad (31)$$

We see that the "original" $\bar{u}_3 - \bar{u}_4$ term has both charge and spin components, but the extra term has only the spin component and obviously can be interpreted as *an exchange of dynamic antiferromagnetic spin fluctuations*. Note the importance of the distinction between u_{3a}^{eff} and u_{3b}^{eff} ($u_{3a}^{eff} = 0.5u_{3b}^{eff}$). If we didn't split u_3 into two *different* components, the additional pairing term would have both spin and charge components.

The term $u_{3b}^{eff}(k - p)$ contains an extra power of $\bar{u}$ compared to the direct $\bar{u}_3 - \bar{u}_4$ term, but, on the other hand, is enhanced at small $k - p$. To see whether $u_{3b}^{eff}(k - p)$ is relevant for s^+ pairing, we need to average (31) over the FS to get s^+ harmonic of the interaction $\Gamma^{s^+} = < \Gamma >_{FS}$. Using $|\mathbf{k} - \mathbf{p}| = 2k_F \sin\theta/2$ and integrating over θ we find that very near SDW transition angular integral is confined to small θ, where Eq. (29) is valid (c.f. Ref.[72]). We then obtain right at the SDW transition

$$\Gamma_{\alpha\beta,\gamma\delta}^{s^+}(k, -k, p, -p) = \frac{1}{2}(\bar{u}_3 - \bar{u}_4)(\delta_{\alpha\beta}\delta_{\gamma\delta} - \sigma_{\alpha\beta}\sigma_{\gamma\delta})$$
$$- C\exp\left[-\frac{2}{(\bar{u}_1 + \bar{u}_3)}\right]\frac{E_F}{|\omega|}\sigma_{\alpha\beta}\sigma_{\gamma\delta} \qquad (32)$$

where $C = O(1)$. We see that the spin-fluctuation contribution to the pairing vertex is exponentially small at weak coupling, but contains $1/\omega$. To compare relative strength of regular and spin-fluctuation contributions, we take $\omega \sim T$ and use for T the solution without spin-fluctuation contribution $T = T_{SC}^{s^+} \sim E_F e^{-1/(\bar{u}_3 - \bar{u}_4)}$. We

then obtain that at such T, spin fluctuation contribution contains extra

$$\exp\left[-\left(\frac{2}{(\bar{u}_1+\bar{u}_3)}-\frac{1}{(\bar{u}_3-\bar{u}_4)}\right)\right] \qquad (33)$$

At small coupling, this is an exponentially small factor. We see therefore that the spin-fluctuation contribution to the pairing is present, but at weak coupling it is exponentially small compared to the regular term in the irreducible vertex, even if we bring the system to a SDW transition point. This implies that the residual coupling between SDW and SC channels does not change the system behavior at weak coupling – – SDW and superconductivity remain competing orders, each develops independent on the other. In other words, s^+ pairing at weak coupling is *not* mediated by spin fluctuations but comes from a direct pair hopping from one Fermi pocket to the other. Spin fluctuation contribution well may become dominant at moderate/strong coupling, but this regime is beyond the scope of the present paper.

Note the crucial role of the dynamics in our consideration. If the magnetically-mediate interaction was purely static, the spin-fluctuation term in (32) would scale as $\sqrt{u_{3b}(0)}$ and eventually become dominant near an SDW transition, when the divergence of $u_{3b}(0)$ overshadows the smallness of the overall factor. The presence of the dynamical component in magnetically-mediated pairing term keeps this term finite even when $u_{3b}(0)$ diverges.

VI. CONCLUSIONS

To conclude, in this paper we presented weak-coupling, Fermi liquid analysis of density-wave and superconducting instabilities in $Fe-$pnictides. We modeled pnictides by a low-energy model of interacting electrons near small hole and electron FS located near $(0,0)$ and $\mathbf{Q}=(\pi,\pi)$ in the folded BZ. The interaction Hamiltonian contains five terms: intra-pocket repulsions u_4 and u_5 (which we set equal), inter-pocket density-density interaction terms u_1 and u_2, and a term u_3 which describes a pair hopping from one pocket to the other. We assumed that the bare interactions $u_i^{(0)}$ are positive and do not depend on a position of a fermion on either of the FS.

We first considered energies between the bandwidth $W \sim 2eV$ and the Fermi energy $E_F \sim 0.1eV$. We demonstrated that particle-hole and particle-particle channels are indistinguishable at these energies, and that all five couplings remain constants and logarithmically flow towards a fixed point with extended symmetry (identified as $SO(6)$ in Ref.[65]). In one-loop approximation which we used, the flow is described by parquet RG equations. In the process of the RG flow, the pair-hopping term and the direct inter-pocket interaction term increase, while intra-pocket interaction u_4 decreases, passes through zero and becomes negative below some energy scale. The interaction u_2 also increases but becomes progressively smaller than other interactions. We argued that the RG flow favors superconductivity: even if the bare couplings are such that the bare pairing interaction is repulsive in all channels, the interaction in the extended $s-$wave pairing channel (s^+) becomes attractive once the renormalized u_3-u_4 becomes positive. This definitely happens under RG because u_4 eventually becomes negative. The order parameter in the s^+ channel is a constant on both hole and electron FS, but changes sign between them.

The $SO(6)$ fixed point is reached at an energy (temperature) when $u^* \log W/E = 1$, where u^* is a linear combination of five bare couplings. At this energy, all couplings diverge, and a Fermi liquid normal state becomes unstable against the development of a six-component order parameter, whose (equivalent) components are SDW, orbital CDW, and s^+ SC. It would be extremely interesting if pnictides displayed this behavior, but this scenario is realized only if $u^* \log W/E = 1$ occurs at $E > E_F$.

Both magnetic and superconducting instabilities in the pnictides occur at $T << E_F$, and we argued that more likely scenario for this materials is that $u^* \log W/E < 1$ down to $E \sim E_F$, and the instabilities are the results of further renormalizations at energies smaller than E_F. We considered the flow of the couplings at these energies and found that the system behavior changes qualitatively: SDW, CDW, and SC channels decouple, and each develops its own order at an energy (temperature) determined by the corresponding couplings at $E = E_F$. We found that for a near-perfect nesting, the instability at the highest energy is towards a conventional SDW order. When doping increases and the nesting becomes less perfect, the first instability eventually becomes a SC instability in the s^+ channel. The transition towards an orbital CDW order (a CDW order with an imaginary order parameter) occurs only slightly below a SDW transition and, in principle, CDW fluctuations should be observable.

Finally, we addressed the issue whether the pairing near a SDW instability can be viewed as mediated by spin fluctuations. To first order in the couplings, the pairing interaction comes directly from the pair hopping and has both charge and spin component. We explicitly demonstrated that the residual coupling between particle-hole and particle-particle channels at energies below E_F gives rise to an additional pairing component, which near an SDW instability reduces to the exchange by spin fluctuations. However, we found that, even at the SDW transition point, this additional interaction is exponentially small compared to a direct pair hopping term. As a result, at weak coupling, the pairing *does not* come from spin-fluctuation exchange. Spin-fluctuation mechanism may, indeed, become dominant at moderate/strong coupling, but to verify this one has to extend the present approach to $u_i^{(0)} \geq 1$.

VII.   ACKNOWLEDGMENT

[1] M.R. Norman, Physics **1**, 21 (2008); C. Xu and S. Sachdev, Nature Physics 4, 898 (2008).

[2] Y. Kamihara, T. Watanabe, M. Hirano, and H. Hosono, J. Am. Chem. Soc. **130** 3296 (2008).

[3] X.H. Chen *et al*, Nature **453** 761 (2008).

[4] G.F. Chen *et al*, Phys. Rev. Lett. **100** 247002 (2008).

[5] Z.-A. Ren *et al*, arXiv:0803.4283 .

[6] M. Rotter, M. Tegel and D. Johrendt, arXiv:cond-mat/0805.4630 (2008).

[7] X.C.Wang *et al.*, arXiv:0806.4688v3 (unpublished).

[8] F.-C. Hsu *et al.*, Proc. Nat. Acad. Sci. **105** 14262 (2008).

[9] J. Dong *et al*, Europhys. Lett. **83**, 27006 (2008).

[10] C. de la Cruz *et al*, Nature **453**, 899 (2008).

[11] T. Nomura *et al*, arXiv:0804.3569 .

[12] H.-H. Klauss *et al*, Phys. Rev. Lett. **101**, 077005 (2008).

[13] Q. Si, and E. Abrahams, Phys. Rev. Lett. **101**, 076401 (2008).

[14] M. Daghofer *et al*, Phys. Rev. Lett. 101, 237004 (2008); A. Moreo, M. Daghofer, J. A. Riera, E. Dagotto, arXiv:0901.3544.

[15] F. Ma, and Z.-Y. Lu, Phys. Rev. B **78**, 033111 (2008).

[16] M. M. Parish, J. Hu, B. A. Bernevig, Phys. Rev. B 78, 144514 (2008).

[17] Q. Si, E. Abrahams, J. Dai, J-X Zhu, arXiv:0901.4112.

[18] S. Lebègue, Phys. Rev. B **75**, 035110 (2007); M.M. Korshunov, and I. Eremin, Phys. Rev. B **78**, 140509(R) (2008).

[19] D. Singh and M.-H. Du, Phys. Rev. Lett. **100**, 237003 (2008).

[20] L. Boeri, O.V. Dolgov, and A.A. Golubov, Phys. Rev. Lett. **101**, 026403 (2008).

[21] I.I. Mazin, D.J. Singh, M.D. Johannes, and M.H. Du, Phys. Rev. Lett. **101**, 057003 (2008).

[22] K. Kuroki *et al*, Phys. Rev. Lett. **101**, 087004 (2008).

[23] K. Haule, J. H. Shim, G. Kotliar, Phys. Rev. Lett. 100, 226402 (2008); J. H. Shim, K. Haule, G. Kotliar, arXiv:0809.0041.

[24] C. Liu *et al.*, Phys. Rev. Lett. **101**, 177005 (2008); T. Kondo *et al*, arXiv:0807.0815 .

[25] D.V. Evtushinsky *et al.*, arXiv:0809.4455 .

[26] D. Hsieh *et al.*, arXiv:0812.2289 .

[27] H. Ding *et al.*, arXiv:0812.0534 .

[28] A.I. Coldea, et.al., Phys. Rev. Lett. **101**, 216402 (2008).

[29] S. E. Sebastian *et al*, J. Phys.: Condens. Matter 20 422203 (2008).

[30] J. Yang *et al*, arXiv:0807.1040.

[31] A. Chubukov, D. Efremov and I. Eremin, Phys. Rev. B , **78**, 134512 (2008).

[32] M.T. Rice, Physical Review B **2**, 3619 (1970).

[33] N. Kulikov and V.V.Tugushev, Sov. Phys. Usp. **27**, 954 (1984), [Usp.Fiz.Nauk **144** 643 (1984)] and references therein.

[34] L.V. Keldysh and Yu.V. Kopaev, Sov. Phys.–Sol. State Phys. **6**, 2219 (1965); J. De Cloizeaux, J. Phys. Chem. Sol. **26**, 259 (1965); B.I. Halperin and M.T. Rice, Sol. State Phys. **21**, 125 (1968).

[35] V. Cvetkovic and Z. Tesanovic, arXiv.org:0808.3742 (2008). See also V. Stanev, J. Kang, and Z. Tesanovic, Phys. Rev. B 78, 184509 (2008).

[36] V. Barzykin and L.P. Gorkov, JETP Lett. **88**, 142 (2008).

[37] S. Graser, T. A. Maier, P. J. Hirschfeld, D. J. Scalapino, arXiv:0812.0343 .

[38] S.-L. Yu, J. Kang, and J.-X. Li, arXiv:0901.0821 .

[39] M.M. Korshunov and I. Eremin, Phys. Rev. B **78**, 140509(R) (2008).

[40] A.B. Vorontsov, M.G. Vavilov, and A.V Chubukov, arXiv:0812.2469.

[41] L. Boeri, O. V. Dolgov, A. A. Golubov, Phys. Rev. Lett. **101**, 026403 (2008).

[42] Y.Yanagi,Y. Yamakawa, and Y. Ono, J. Phys. Soc. Jpn. **77** 123701 (2008); H. Ikeda, J. Phys. Soc. Jpn. **77**, 123707 (2008)

[43] Y. Bang, H.-Y. Choi, and H. Won, arXiv:0808.3473 .

[44] Fa Wang *et al*, arXiv:0807.0498; F. Wang *et al*, arXiv:0805.3343; F. Wang *et al*, arXiv:0807.0498.

[45] K. Seo, B. A. Bernevig, J. Hu, Phys. Rev. Lett. 101, 206404 (2008)

[46] In the diagrammatics, RPA corresponds to summing up separately ladder series of diagrams and bubbler series of diagrams. To study the flow of the couplings one has to add renormalizations in the direction transverse to either of these channels, i.e., perform parquet-type RG calculations (see text).

[47] T. Y. Chen *et al*, Nature **453**, 1224 (2008).

[48] A.D. Christianson *et al.*, Nature **456**, 930 (2008); M.D. Lumsden *et al.*, arXiv:0811.4755 .

[49] T.A. Maier and D.J. Scalapino, Phys. Rev. B **78**, 020514(R) (2008).

[50] Y. Nakai *et al*, J. Phys. Soc. Jpn. **77**, 073701 (2008); Y. Nakai *et al*, arXiv:0810.3569 .

[51] K. Matano *et al*, Europhys. Lett. **83**, 57001 (2008).

[52] H.-J. Grafe *et al.*, Phys. Rev. Lett. **101**, 047003 (2008).

[53] R.T. Gordon *et al.*, arXiv:0810.2295 ; R.T. Gordon *et al.*, arXiv:0812.3683 ; J.D. Fletcher *et al.*, arXiv:0812.3858 (unpbulished).

[54] K. Hashimoto *et al.*, Phys. Rev. Lett. **102**, 017002 (2009).

[55] D. Parker *et al*, Phys. Rev. B **78**, 134524 (2008).

[56] Y. Senga and H. Kontani, J. Phys. Soc. Jpn. **77**, 113710 (2008)

[57] A.B. Vorontsov, M.G. Vavilov, and A.V Chubukov, arXiv:0901.0719.

[58] P. Ghaemi, F. Wang, and A. Vishwanath, arXiv:0812.0015 (unpublished).

[59] D. Parker and I. Mazin, arXiv:0812.4416 (unpublished); J. Wu and Ph. Phillips, arXiv:0901.0038 (unpublished).

[60] A.V. Chubukov, I. Eremin and M.M. Korshunov, arXiv:0901.2102.

[61] Cenke Xu, Markus Mueller, and Subir Sachdev, Phys. Rev. B 78, 020501(R) (2008); Cenke Xu, Yang Qi, and Subir Sachdev, arXiv:0807.1542.

[62] P. Chandra, P. Coleman, and A.I. Larkin, Phys. Rev. Lett. **64**, 88 (1990).

[63] see. e.g., C. Cao, P.J. Hirschfeld, H.-P. Cheng, Phys. Rev. B **77**, 220506(R) (2008).

[64] Note that our two-band model differs conceptually from the two-band model based on the d_{yz} and d_{xz} orbitals considered by S. Raghu *et al* [Phys. Rev. B **77** 220503(R) (2008)]. Band structure calculations[20] show that not only d_{yz} and d_{xz} orbitals, but all Fe $5d$-orbitals contribute to the bands crossing the Fermi level, and, besides, Fe $5d$-orbitals strongly hybridize with the As p-states. The tight-binding model of the pnictides then should include 8 bands in the unfolded BZ. Our model with two hybridized orbitals and two bands crossing the Fermi level is not related to actual Fe $5d$ and As p -orbitals, and is simply a phenomenological minimal model to describe SDW and superconductivity.

[65] D. Podolsky, H-Y. Kee, Y. B. Kim, arXiv:0812.2907.

[66] A.T. Zheleznyak, V.M. Yakovenko, and I.E. Dzyaloshinskii, Phys. Rev. B **55**, 3200 (1997).

[67] W.L. McMillan, Phys. Rev. **167**, 331 (1968).

[68] J. Wu, P. Phillips, and A.H. Castro-Neto, arXiv:0805.2167.

[69] P.Fulde and R.Ferrell, Phys. Rev. **135** A550 (1964); A. I. Larkin and Y.N. Ovchinnikov, Zh. Eskp. Teor. Fiz. **47** 1136 (1964) [Sov. Phys. JETP **20**, 762 (1965)].

[70] A. M. Tsvelik, private communication

[71] see e.g., M. Eschrig, Advances in Physics, **55**, 47, (2006) and references therein.

[72] A.V. Chubukov, D.L. Maslov, S. Gangadharaiah, and L.I. Glazman, Phys. Rev. Lett. **95**, 026402 (2005); Phys. Rev. B **71**, 205112 (2005); A.V. Chubukov and D.L. Maslov, unpublished.

[73] see, e.g., N. Shah and A. Lopatin, Phys. Rev. B 76, 094511 (2007) and references terein.